Facile synthesis of mesoporous N doped zirconium titanium mixed oxide nanomaterial with enhanced photocatalytic activity under visible light†

Noor Aman,[a] Trilochan Mishra,*[a] Ranjan K. Sahu[b] and J. P. Tiwari[c]

Received 6th May 2010, Accepted 24th August 2010
DOI: 10.1039/c0jm01342k

The present paper deals with a hydrazine mediated synthesis of high surface area and thermally stable N-doped zirconium titanium mixed oxide with enhanced photocatalytic activity towards reduction of selenium (VI) to metallic Se^0 under visible light. Materials were synthesized at pH = 2 by varying the hydrazine concentration and characterized by XRD, TEM, BET method, XPS, Raman spectroscopy and UV-vis solid state spectra. Presence of low amount of zirconium oxide (10 wt%) helps in phase stabilization and maintains the porous structure even at higher calcinations temperature in comparison to that of pure titania. XPS spectrum justifies the presence of nitrogen and Ti^{3+} in the material due to the decomposition reaction of hydrazine. Hydrazine controls the nitrogen content, surface area and the formation of oxygen vacancy in the material. Investigation of metal oxide to hydrazine ratio on the overall surface properties and photocatalytic activity indicates that the 1 : 6 ratio is the optimum composition for the best result. Surface area and pore volume increases to 298 m^2/g and 0.323 cm^3/g. The obtained material (TiZr-6N-400) is found to reduce selenium (VI) to selenium (0) under visible light within only 45 min of reaction. Increased photocatalytic activity under visible light is mostly due to the synergistic effect of substantial nitrogen doping, high surface area and presence of oxygen vacancy.

1. Introduction

Since the discovery of photo-induced water decomposition under UV light[1] TiO_2 has received much attention as a potential photocatalyst for future environmental application. However, pure titania can only work under ultraviolet (UV) light (wavelength $\lambda < 388$ nm) due to its wide band gap of 3.0–3.2 eV, which means only about 4% of the incoming solar energy on the earth surface can be utilized. The development of visible-light photocatalysts, therefore, has become one of the most important topics in photocatalysis research.[2–5] In this regard, the first report of Asahi *et al.* on the band gap reduction of the oxide material by N doping stimulated the researchers for the investigation of nonmetal doped titania photocatalysts. Subsequently many semiconductor photocatalysts based on $TiO_{2-x}M_x$, where M is N,[6–8] C,[9–11] S[12–14] or F,[15,16] have been investigated for practical application under visible/indoor light. Among all, nitrogen doped titania has been exhibited to be an efficient way to extend the absorption of light from the ultraviolet to visible region because the substitutional doping of N for O in the anatase TiO_2 crystal would yield a band gap narrowing. Recently, it is observed that oxygen vacancies created by the N doping play an important role for increasing the visible light absorption.[17] That is why N-doped anatase titania has emerged as the most attractive material for researchers in the last decade.[18,19] In addition, porosity of the photocatalyst is quite important for increasing the catalytic performance of the material. In this context, the synthesis of high surface area anatase spheres[20] with improved photocatalytic activity was reported by hydrolysis of titanium glycolate at reflux conditions. However, loss of high surface area and phase conversion from anatase to rutile above 500 °C is the main concern of most of the titania based materials.[21] Calcination at high temperatures (≥400 °C) is mostly required for crystallization and for achieving effective doping of cations/anions in the lattices of the TiO_2 photocatalyst. Unfortunately, such a high temperature treatment often leads to a loss of surface area due to the grain growth and phase conversion from anatase to rutile. Hence, the photocatalyst retains very low specific surface area after calcination, greatly reducing their light-harvesting capability. So, a lot of effort has been made to stabilize the anatase phase even at high temperature through mixing of low amount of another metal oxide.[22] In this context addition of zirconia and silica to titania has been observed to improve the anatase phase stabilization, surface properties and photocatalytic activities.[22–24] In the last few years ZrO_2 mixed TiO_2 materials have been intensively studied for enhanced photocatalysis.[25,26] It has been proposed that the incorporation of Zr^{4+} in titania increases thermal stability and surface acidity of the material. However for practical application under solar light or indoor illumination, it is appealing to develop a visible light sensitive, high surface area and thermally stable anatase based material. In this regard very limited investigations are reported on the non-metals like F,[27] N[28] and S[29] doped zirconia titania systems. It is understood from the previous studies that the synthesis process, precursors for nitrogen and doping concentration play a decisive role on the surface properties and the photocatalytic activity. In particular, the effect of these variations on the surface and photocatalytic properties of titania

[a]*ACC Division, National Metallurgical laboratory, CSIR, Jamshedpur, 831007, India. E-mail: drtmishra@yahoo.com; Fax: +91 657 234*
[b]*MST Division, National Metallurgical laboratory, CSIR, Jamshedpur, 831007, India*
[c]*FM Division, Central Electrochemical Research Institute, CSIR, Karaikudi, 630006, India*
† Electronic supplementary information (ESI) available: Further figures. See DOI: 10.1039/c0jm01342k

zirconia material is yet to be investigated systematically. Moreover, the use of a reducing agent like hydrazine as a source of nitrogen is also rarely reported. Because of the reducing nature of hydrazine there is a possibility of Ti^{3+} formation which will facilitate the formation of oxygen vacancies in the material. So in the present work we use a simple approach for the synthesis of high surface area, thermally stable N-doped zirconium titanium mixed oxide with enhanced photocatalytic activity towards reduction reactions under visible light employing hydrazine as a source of nitrogen. Presence of a low amount of zirconium oxide (10 wt. %) helps in the phase stabilization and maintains the porous structure even at higher calcination temperatures in comparison to that of pure titania. Besides, the effect of hydrazine to metal oxide ratio on the overall activity is investigated so as to have better understanding on the optimum composition. The obtained material is found to reduce 25 ppm of selenium (VI) to Se(0) within only 45 min under visible light.

2. Experimental

2.1. Material synthesis

Titanium zirconium oxide in the weight ratio of 90 : 10 (TiZr) was synthesized by controlled hydrolysis of titanium and zirconium butoxide at pH 2.0. A mixture of both the metal butoxides in required amount was diluted to 20 ml with n-propanol and slowly added to 100 ml of aqueous solution of pH = 2.0 under stirring at 27 °C. Nitrogen doping was achieved by hydrazine addition to a titanium zirconium oxide suspension and the mixture was kept under stirring for another 12 h. Subsequently the mixture was evaporated slowly up to drying. Oxide to hydrazine molar ratio was varied from 1 : 2 to 1 : 8 so as to understand the effect of hydrazine concentration on the nitrogen doping as well as surface properties of the final material. The obtained N-doped material was calcined at different temperatures for further use. For comparison, N doped pure titania (Ti-6N) with a molar ratio of 1 : 6 was synthesized following the same procedure. Obtained samples are coded according to the hydrazine molar ratio.

2.2. Material characterization

XRD patterns of all the synthesized samples calcined at different temperatures were recorded on a Siemens (model: D-500) semi-automatic diffractometer using Cu Kα and Co Kα radiation source in the range 10 to 80 degrees.

Samples for TEM measurements were prepared by redispersion of the obtained powdered samples in isopropanol and subsequently placing a drop of the colloidal solution on carbon coated copper TEM grid. The film on the TEM grid was allowed to dry prior to the measurement. TEM measurements were performed on a JEOL (2100F field emission TEM) instrument operated at an accelerating voltage of 120 kV.

UV-visible diffused reflectance spectra of all the synthesized materials were recorded on the Shimadzu 2550 spectrophotometer using $BaSO_4$ as the reference material.

Raman spectra of the powdered materials are recorded using Nicolet Almega XR (Thermo) dispersion Raman spectroscopy.

2.3. XPS

X-Ray photoelectron spectroscopy (XPS) was recorded by UHV analysis system (SPECS, Germany) with a Mg Kα monochromatized X-ray source (E = 1253.6 eV). The instrument was operated at a pressure of 6×10^{-9} Torr in the analysis chamber. Photoelectrons were collected with pass energy of 80 eV for surveys, and 20 eV for high-resolution spectra. The binding energies were collected with a reference to the maximum intensity of the C 1s (285.0 eV). Analysis of the spectra was done using CASA XPS software.

2.4. BET surface area and pore size analysis

BET surface area was determined by a N_2 adsorption–desorption method at liquid nitrogen temperature using Nova 4000e (Quantachrome, USA). Prior to adsorption–desorption measurements, the samples were degassed at 393 K at 10^{-3} Torr for 5 h.

2.5. Photocatalytic activity

Prepared materials after calcination at different temperatures were used as photocatalysts for the reductive removal of selenium (VI). A stock solution of selenium was prepared by dissolving the required amount of sodium selenate salts in double distilled water. All the photocatalytic experiments were carried out in a 200 ml capacity three necked glass reactor fitted with a 125 W high pressure Hg lamp under magnetic stirring. A constant reaction temperature was maintained through water circulation in the outer jacket of the glass reactor. All the experiments were performed in the presence of air at atmospheric pressure. Initial concentration of metal ions was maintained at 25 ppm in each experiment. Formic acid (100 ppm) is used as the hole scavenger for Se (VI) reduction experiment. During the reaction selenium (VI) is converted to red selenium metal and deposited on the catalyst surface. For kinetic experiments around 10 ml of the reaction mixture is pipetted out at different intervals of reaction time. From the reaction mixture a solid catalyst was separated by filtration or centrifugation. Selenium (VI) concentration in the solution after and before reaction was estimated by atomic absorption spectroscopy (AAS).

3. Result and discussion

3.1. Textural properties

The XRD pattern (Fig. 1) reveals that the TiZr-6N material calcined up to 600 °C is present in anatase form whereas the formation of rutile phase starts even at 500 °C calcination temperature in the case of Ti-6N (ESI,† Fig. S1). This indicates that the presence of zirconia inhibits phase transformation and crystal growth in the solids. A similar observation was also observed in case of zirconia and silica mixed titania materials.[22] Absence of any extra peaks for a zirconia phase indicates the homogenous incorporation of zirconium in the titania matrix. So the stabilization of nanocrystalline anatase at higher calcination temperatures is encouraging as it has been considered as the most photoactive form of titania. Moreover, TiZr-6N shows a very low amount of rutile phase even after calcinations at 800 °C

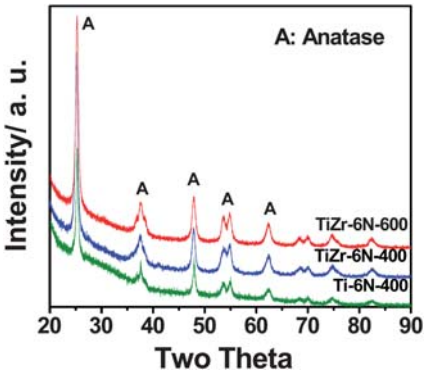

Fig. 1 XRD of different synthesized materials recorded using copper source.

indicating the increased thermal stability of the anatase phase due to the presence of Zr ions. These results are consistent with the results obtained from the selective area diffraction (SAD) pattern of the material. A ring type SAD pattern in association with the microstructure obtained from TEM experiment justifies the formation of nanoparticles in the range 13–20 nm. It is clearly noted that there is a difference in the shape and size of the particles in the case of N doped and undoped material (Fig. 2). The pure TiZr material shows a nearly spherical shape of the particles having an average diameter of 50 nm. Of course these spherical particles are composed of so many smaller particles. Mostly the addition of hydrazine increases the particle aggregation due to the increased pH as observed in Fig. 2b. N_2 adsorption–desorption isotherms (ESI,† Fig. S2) of all the materials are of type IV which is characteristic of mesoporous materials. However a hysteresis loop with a triangular shape and steep desorption branch, observed in case of TiZr-6N-400, suggests the presence of pores with narrow mouths. It is observed that the BJH pore size distribution (Fig. 3) shifts towards a narrow range with nitrogen doping. Out of all the materials TiZr-6N-400 and Ti-6N show the highest (298 m^2/g) and lowest surface area (Table 1), respectively. During subsequent calcination at 600 and 800 °C, the surface area of TiZr-6N decreases to 183 and 102 m^2/g respectively. However, the surface area drastically decreases in case of Ti-6N with increasing calcination temperature. So it can be concluded from the XRD and surface area measurements that Zr ions stabilize TiO_2 in the anatase phase with a reasonably high surface area even at an 800 °C calcination temperature. Fig. 4 shows the Raman spectra of the N-doped and undoped materials. Clear peaks at 144 (E_g), 397 (B_{1g}), 517 ($A_{1g} + B_{1g}$) and 640 cm^{-1} (E_g) typically match with the

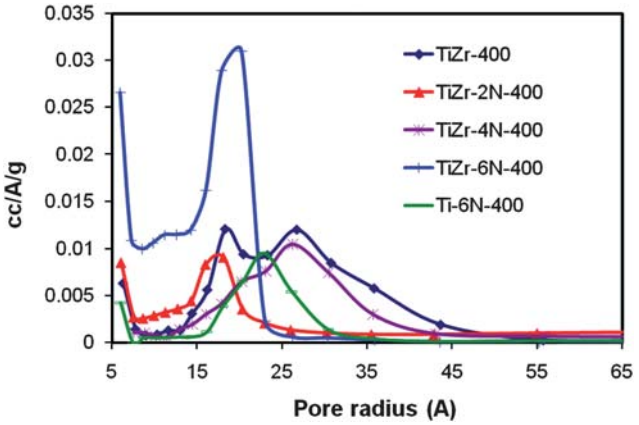

Fig. 3 Pore size distribution of synthesized materials with varying hydrazine amounts.

Table 1 Surface area, pore volume of N-doped materials calcined at different temperatures

Materials	Calcination temperature (°C)	BET surface area (m^2/g)	Pore volume (cm^3/g)
TiZr	400	130	0.265
TiZr-2N	400	128	0.263
TiZr-4N	400	186	0.277
TiZr-6N	400	298	0.323
TiZr-8N	400	235	0.292
TiZr-6N	600	186	0.278
TiZr-6N	800	102	0.208
Ti-6N	400	68	0.152
Ti-6N	600	32	0.124

Raman active modes for the anatase phase. Similar to the XRD results, Raman spectra also support the homogeneous distribution of zirconium in the anatase lattice without forming any separate phase. A clear and strong peak at 144 cm^{-1} indicates the high crystallinity of the materials. A minor peak shift is observed in the case of TiZr-6N in comparison to that of pure titania. In addition, peak broadening is also observed in all the spectra. Peak broadening is mostly due to the formation of nanoparticles.

3.2. Effect of hydrazine on surface properties

It is found that with the increasing metal oxide to hydrazine ratio up to 1 : 6, surface area of the material increases. However further increasing the metal oxide to hydrazine ratio to 1 : 8,

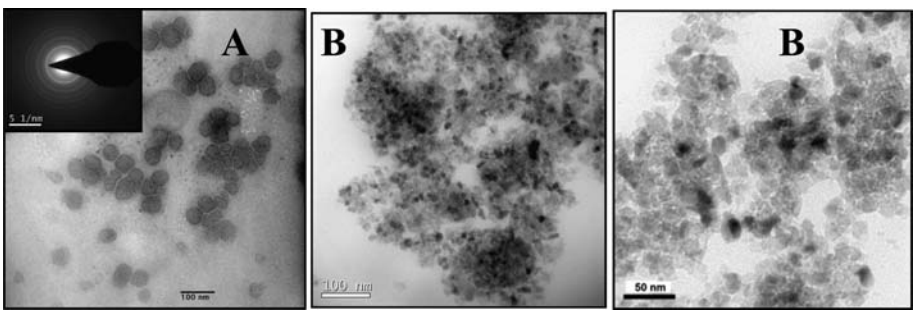

Fig. 2 TEM micrographs of (a) TiZr and (b) TiZr-6N materials.

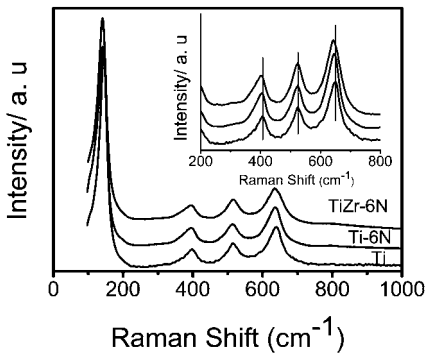

Fig. 4 Raman spectra of titania and the nitrogen doped materials.

surface area and the pore volume decreases. Surface area is marginally decreased in the case of TiZr-2N with a low hydrazine concentration. In this case the amount of hydrazine is insufficient to create porosity during decomposition under heat treatment. When the hydrazine amount is increased above 1 : 2, porosity of the calcined material increases due to the decomposition of entrapped hydrazine. Surface area and pore volume increases with the increasing hydrazine amount to 298 m^2/g and 0.323 cm^3/g, respectively. Therefore, the hydrazine amount is crucial in the synthesis process to control nitrogen doping and to create porous structures. Porosity of a material is crucial for enhanced catalytic activity as it increases the number of available active sites. It is known that hydrazine decomposes to form ammonia, nitrogen and hydrogen gas under heat treatment as shown below.

$$N_2H_4 \rightarrow 4NH_3 + N_2$$

$$4NH_3 + N_2H_4 \rightarrow 3N_2 + 8H_2$$

Earlier Domen *et al.*[30] demonstrated the use of ammonia to introduce nitrogen in the oxide lattice at high temperature. Indeed the recent study by Mapa *et al.*[31,32] suggests that the *in situ* ammonia formation through urea decomposition is the reason for N doping in ZnO. So in the present case *in situ* generated ammonia from hydrazine decomposition within the material

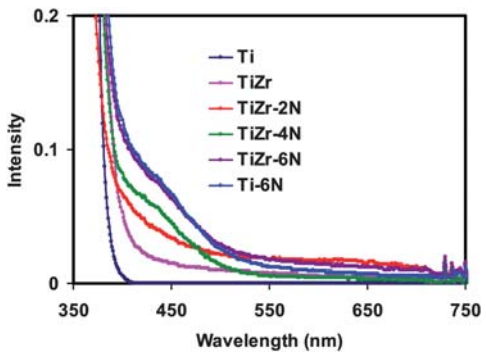

Fig. 5 UV-Vis spectra of different nitrogen doped materials.

helps in both nitrogen doping and creation of porous structure. A low surface area (68 m^2/g) of N doped titania calcined at 400 °C indicates that the only hydrazine decomposition during calcinations may not be responsible for the stabilization of porous structure. Rather the presence of zirconium with titania is responsible in stabilizing the porous structure even at high calcination temperature. That is why pure TiZr also shows a comparatively high surface area of 130 m^2/g. So it can be concluded that the presence of zirconium not only helps in stabilizing the anatase phase but also helps to maintain the porous structure even at high calcination temperature. UV-Vis diffuse reflectance spectra of different synthesized materials calcined at 400 °C are presented in Fig. 5. Visible light absorption of the material increases with the increasing hydrazine content. Both TiZi-6N and Ti-6N materials after calcination at 400 °C are yellow in colour and significantly absorb in the visible light range up to 530 nm. This shift in the absorption band of the synthesized materials indicates the nitrogen doping into the oxide matrix. In the absorption spectra of N doped materials a continuous but slow decreasing band is observed without any steep absorption edge in the visible light region. Such shoulder type absorption might be due to the defects in the lattice. It is also understood that defects created by oxygen vacancies can induce colour and also increase the visible light absorption.[33]

3.2.1. Surface chemical properties. The above results signify that the incorporation of nitrogen in the presence of Zr^{4+} has a significant contribution towards the surface chemical environment though the anatase phase is retained. Our O1s spectra (Fig. 6) show the presence of a small peak at 532 eV in addition to the main peak at ~530 eV particularly in the case of N doped materials. The deconvolution of the spectra clearly shows the presence of a small but significant peak at 532 eV. In the literature this peak is assigned to the presence of a surface hydroxyl group by different authors.[27] On the other hand, Chen *et al.*[18] attributed the same peak to the N doping of the titania matrix. More recently, it was observed that the same peak is observed in a titania material having oxygen vacancy.[34] Due to the creation of oxygen vacancies the adjacent oxygen atom experiences less electron density in comparison to other lattice oxygen atoms. Hence the peak due to these oxygen atoms shifts towards the higher binding energy. This usually results as a shoulder at around 532 eV in addition to the original oxygen peak. At the same time it is well understood that N doping facilitates the formation of oxygen vacancies[17,33] in titania materials which accounts for the enhancement in the photocatalytic activity under visible light. Indeed it is not easy to assign the same peak (532 eV) to the exact contribution in the material. However, the contribution of oxygen vacancies can not be ruled out. The XPS data of Ti2p presented in Fig. 7a and b show some interesting observations. In the case of both the nitrogen doped materials two peaks at 459.2 and 464.9 eV are clearly visible representing $Ti2p_{3/2}$ and $Ti2p_{1/2}$. In the case of Ti-6N, there is a clear shoulder observed at 457 eV indicating the presence of an extra peak in addition to the original one at 459.7 ev. This additional peak indicates the presence of Ti^{3+} in the material. Mostly the used hydrazine which is a reducing agent is responsible for the formation of Ti^{3+}. Convolution of the Ti 2p spectrum of TiZr-6N also shows the presence of a small peak at 457 eV. On the basis of

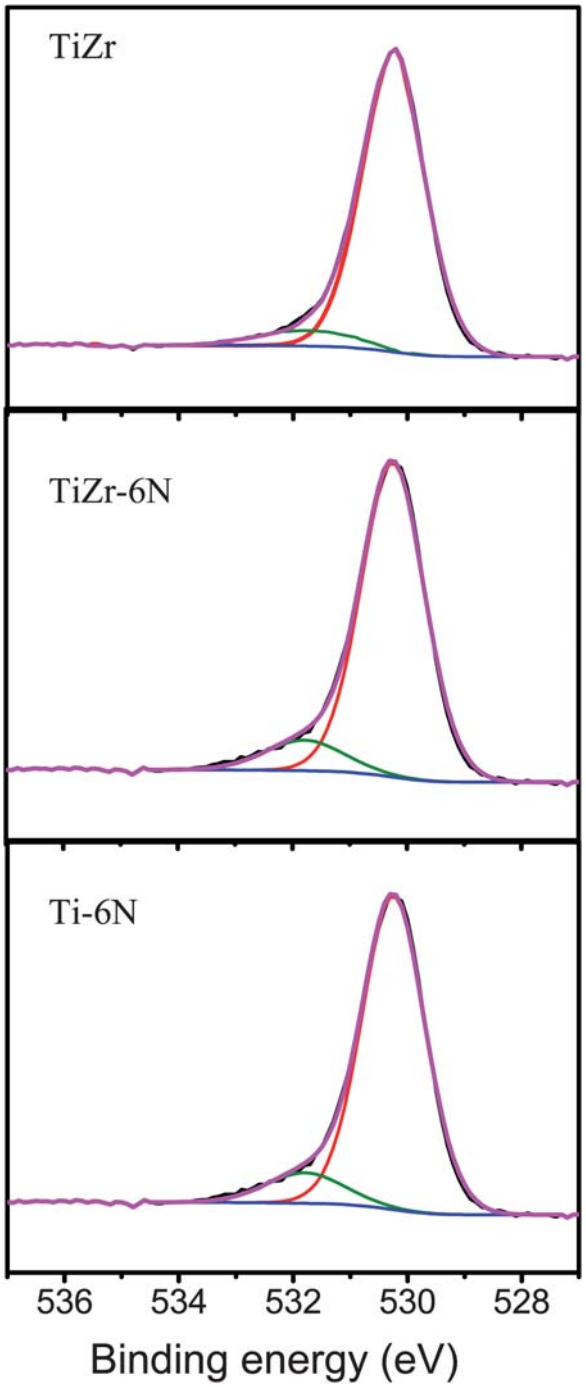

Fig. 6 Comparative O1s XPS spectra of TiZr, Ti-6N and TiZr-6N.

the area of the peak Ti^{3+} present in Ti-6N and TiZr-6N is 21.2 and 9.4% respectively. So it can be inferred that the presence of zirconium controls the reductive formation of Ti^{3+} in the material. On the other hand assignment of a 532 eV peak of oxygen 1s to the oxygen vacancy is supported by the fact that the presence of Ti^{3+} is a major source of oxygen vacancies in the material. In this regard Ti-6N will have more oxygen vacancies than TiZr-6N considering the amount of Ti^{3+} present in the material. However it is not possible here to quantitatively estimate the amount of oxygen vacancies in the material.

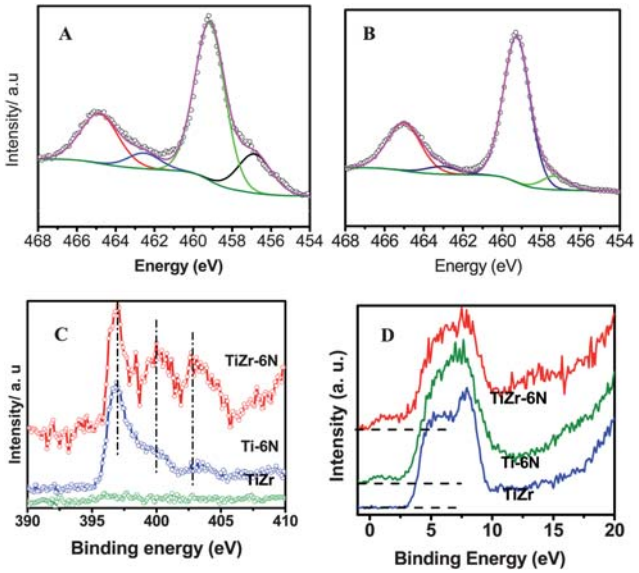

Fig. 7 Comparative presentation of XPS data (a) Ti2p spectra of Ti-6N, (b) Ti2p spectra of TiZr-6N, (c) N1s spectra and (d) valency band spectra.

The N1s XPS spectrum (Fig. 7c) in the range 397–403 eV again signifies that the nitrogen is doped into the oxide lattice[35] in three different forms. Fig. 7c shows the presence of three different peaks with varying intensities in the case of both N doped materials. The presence of peaks at 397 and 400.5 eV signifies the doping in the matrix and the formation of NO species, respectively in the material. Still another low intensity peak is observed at 402.5 eV which is somewhat prominent in the case of TiZr-6N. This peak is rarely observed in N doped materials. It is observed in between the standard position of NO and NO_2 (405 eV) so it can be due to the formation of more electropositive NO type species. However the assignment of the nitrogen 1s peak in the XPS spectra is under debate in the literature. So without going to the exact species formed here we can say a significant amount of N is doped through the present process using hydrazine. In addition, a clear diffused electronic state of TiZr-6N is observed as a shoulder (Fig. 7d) above the valency band edge of pure titania. This again confirms the doping of nitrogen in the crystal lattices[36] which lowers the oxidation potential for visible light applications. Interestingly, the small peak above the valency band can also be due to the oxygen vacancy[33] present in the material. This additional electron density state explains the red shifts observed in the UV-Vis spectra. However it is well agreed that N doping in the crystal induces photocatalytic activity under visible light illumination which is not observed in case of pure titania. Recently it is observed that titania with oxygen vacancies can perform as a better photocatalyst under visible light.[34] Moreover nitrogen doping helps in the creation of the oxygen vacancy. So it is clear that N doping itself helps in the visible light absorption as well as the creation of oxygen vacancies in the material. From the above discussion it is clear that the synthesized material contains doped nitrogen as well as oxygen vacancy. However, at present it is very difficult to separate the contribution of oxygen vacancies from the N doping in the crystal lattice to have a quantitative contribution of both the effects.

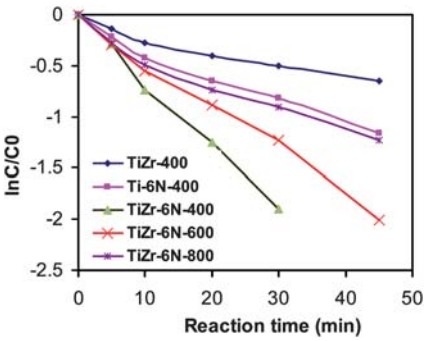

Fig. 8 Plot of ln C/C_0 *vs.* reaction time for selenium (VI) reduction over different materials under visible light.

3.3. Photocatalytic performance

To evaluate the photocatalytic performance we use reduction of selenium (VI) to selenium (0) in aqueous media as a test reaction. Preliminary experiments show that the use of hole scavengers like formic acid substantially increases the reduction activity. During the reduction reaction the catalyst became red in colour due to the deposition of red selenium (0). The photocatalytic reaction of a 25 ppm selenium (VI) aqueous solution in the presence of 100 ppm of formic acid was carried out with time and presented in Fig. S3 (ESI†) for all the materials. It is well observed that with the increasing hydrazine amount in the material photocatalytic performance increases up to 1 : 6 and thereafter decreases. Complete conversion of Se(VI) to Se(0) is observed in 45 min of reaction with TiZr-6N.

The photocatalytic reduction activity of TiZr-6N calcined at different temperatures is compared with Ti-6N under visible light in the presence of 100 ppm of formic acid. Fig. 8 indicates that 100% reduction of Se (VI) to Se (0) within 45 min of reaction is possible over the TiZr-6N-400 material whereas Ti-6N-400 can reduce only 69% of Se (VI) during the same time period. Catalytic activity is quite dependent on the surface area of a material as it facilitates the reactant to reach the available active sites. High porosity increases the number of available active sites of a catalyst thereby increasing the catalytic activity. Therefore the higher photocatalytic activity can be correlated to the high porosity of the nitrogen doped TiZr materials. In addition, the selenium reduction reaction is quite dependent on the available surface area as reduced Se (0) is deposited on the catalyst surface thus reducing the number of available sites. So the drastic enhancement of photocatalytic activity under visible light over TiZr-6N can be attributed to the substantially higher surface area of TiZr-6N in comparison to N-doped titania having surface area of 68 m^2/g. Based on the presence of Ti^{3+}, the amount of oxygen vacancies is expected to be higher in the case of Ti-6N. However, the catalytic activity demonstrated by Ti-6N is not encouraging. A high amount of Ti^{3+} presence may promote the formation of TiN species which are not good photocatalysts. This may be the reason for the decreased visible light activity of Ti-6N in addition to low surface area. So this can be concluded that formation of low amount of Ti^{3+} is preferred for the enhanced visible light activity. UV-Vis spectra show that the visible light absorption capacity of the material increases with the increasing hydrazine amount. Again it confirms that both the materials (TiZr-6N-400 and Ti-6N-400) have a similar visible light harvesting capability. In particular, a high surface area of the material creates a higher number of accessible active sites for the reaction and hence the present material performs better than Ti-6N-400 particularly under visible light illumination. It was also understood that the doping of nonmetal and metal in the titania matrix can induce visible light driven photocatalysis by creation of defects. Therefore the additional role of extrinsic absorption bands created by the oxygen vacancies of the catalyst can not be ruled out in the present study. Recently it was reported that oxygen vacancies can enhance the visible light mediated catalytic activity to a very high level.[34] Therefore the enhanced photocatalytic reduction and oxidation activity of TiZr-6N-400 under visible light can be attributed to the synergistic effect of high surface area, oxygen vacancy and substantial N doping. So it is important to study the exact contribution of the oxygen vacancy as well as the non-metal doping separately for better understanding of the photocatalyst.

Conclusion

In summary, the present report describes the synthesis of high surface area, thermally stable N-doped titanium zirconium oxide materials with comparatively high photocatalytic activity towards selenium (VI) reduction reaction under visible light illumination. XRD and Raman spectra confirm the stabilization of the anatase phase even at 800 °C calcination. The amount of hydrazine plays an important role in nitrogen doping as well as the formation of a porous structure in the material. Surface area and pore volume increases with the increasing hydrazine amount to 298 m^2/g and 0.323 cm^3/g, respectively. The amount of nitrogen doping and the visible light absorption capacity of the material increase with the increasing hydrazine amount up to an optimum value. Nitrogen doped titania zirconia material exhibits high surface area and enhanced visible light mediated photocatalytic activity in comparison to nitrogen doped pure titania. XPS analysis confirms the presence of Ti^{3+} in N doped materials which creates oxygen vacancies also. Complete reduction of 25 ppm of selenium (VI) to metallic red Se^0 is possible within only 45 min over TiZr-6N-400. The enhanced photocatalytic reduction activity of nitrogen doped titania zirconia mixed oxide under visible light can be attributed to the synergistic effect of high surface area, presence of oxygen vacancies and substantial N doping. Enhanced visible light photocatalysis results of the synthesized materials may generate significant interest for waste water treatment under visible/solar light. It is also important to study the exact contribution of the oxygen vacancy as well as the non-metal doping for better understanding of the photocatalyst.

Acknowledgements

Authors are thankful to the Director, NML for his encouragement and permission to publish the work. We are also thankful to the DST for providing financial support in the form of project under green chemistry scheme. One of the authors Noor Aman is thankful to the CSIR for providing senior research fellowship.

References

1 A. Fujishima and K. Honda, *Nature*, 1972, **238**, 37.
2 Z. G. Zou, J. H. Ye, K. Sayama and H. Arakawa, *Nature*, 2001, **414**, 645.
3 M. Gratzel, *Nature*, 2001, **414**, 338.
4 R. Asahi, T. Morikawa, T. Ohwaki, K. Aoki and Y. Taga, *Science*, 2001, **293**, 269.
5 S. Khan, M. Al-Shahry and W. B. Ingler, *Science*, 2002, **297**, 2243.
6 C. Burda, Y. Lou, X. Chen, A. C. S. Samia, J. Stoutand and J. L. Gole, *Nano Lett.*, 2003, **3**, 1049.
7 T. Lindgren, J. M. Mwabora, E. Avendano, J. Jonsson, A. Hoel, C. G. Granqvist and S. E. Lindquist, *J. Phys. Chem. B*, 2003, **107**, 5709.
8 S. Sakthivel and H. Kisch, *ChemPhysChem*, 2003, **4**, 487.
9 H. Irie, Y. Watanabe and K. Hashimoto, *Chem. Lett.*, 2003, **32**, 772.
10 Y. Choi, T. Umebayashi, S. Yamamoto and S. Tanaka, *J. Mater. Sci. Lett.*, 2003, **22**, 1209.
11 S. Sakthivel and H. Kisch, *Angew. Chem., Int. Ed.*, 2003, **42**, 4908.
12 T. Umebayashi, T. Yamaki, H. Itoh and K. Asai, *Appl. Phys. Lett.*, 2002, **81**, 454.
13 T. Umebayashi, T. Yamaki, S. Tanala and K. Asai, *Chem. Lett.*, 2003, **32**, 330.
14 J. C. Yu, W. K. Ho, J. G. Yu, H. Y. Yip, P. K. Wong and J. C. Zhao, *Environ. Sci. Technol.*, 2005, **39**, 1175.
15 D. Li, H. Haneda, N. K. Labhsetwar, S. Hishita and N. Ohashi, *Chem. Phys. Lett.*, 2005, **401**, 579.
16 W. Ho, J. C. Yu and S. Lee, *Chem. Commun.*, 2006, 1115.
17 C. Feng, Y. Wang, Z. Jin, J. Zhang, S. Zhang, Z. Wu and Z. Zhang, *New J. Chem.*, 2008, **32**, 1038.
18 X. Chen, Y. Lou, A. C. S. Samia, C. Burda and J. L. Gole, *Adv. Funct. Mater.*, 2005, **15**, 41.
19 J. Wang, W. Zhu, Y. Zhang and S. Liu, *J. Phys. Chem. C*, 2007, **111**, 1010.
20 L.-S. Zhong, J.-S. Hu, L.-J. Wan and W.-G. Song, *Chem. Commun.*, 2008, 1184.
21 A. S. Deshpande, D. G. Shchukin, E. Ustinovich, M. Antonietti and R. A. Caruso, *Adv. Funct. Mater.*, 2005, **15**, 239.
22 T. Mishra, J. Hatti, Noor Aman, R. K. Jana, M. Gunjan and B. Mahato, *J. Colloid Interface Sci.*, 2008, **327**, 377.
23 J. Lukac, M. Klementova, P. Bezdicka, S. Bakardjieva, J. Subrt, L. Szatmary, Z. Bastl and J. Jirkovsky, *Appl. Catal., B*, 2007, **74**, 83.
24 C. Anderson and A. J. Bard, *J. Phys. Chem. B*, 1997, **101**, 2611.
25 M. D. Hernandez-Alonso, J. M. Coronado, B. Bachiller-Baeza, M. Fernandez-Gracia and J. Soria, *Chem. Mater.*, 2007, **19**, 4283.
26 W. Zhou, *Nanotechnology*, 2008, **19**, 35610.
27 S. Liu, J. Yu and S. Mann, *J. Phys. Chem. C*, 2009, **113**, 10712.
28 X. Wang, J. C. Yu, Y. Chen, L. Wu and X. Fu, *Environ. Sci. Technol.*, 2006, **40**, 2369.
29 G. Tian, K. Pan, H. Fu, L. Jing and W. Zhou, *J. Hazard. Mater.*, 2009, **166**, 939–944.
30 K. Maeda, K. Teramura, D. Lu, T. Takata, N. Saito, Y. Inoue and K. Domen, *Nature*, 2006, **440**, 295.
31 M. Mapa and C. S. Gopinath, *Chem. Mater.*, 2009, **21**, 351.
32 M. Mapa, K. Sivaranjani, D. S. Bhange, B. Saha, P. Chakraborty, A. K. Viswanath and C. S. Gopinath, *Chem. Mater.*, 2010, **22**, 565.
33 J. Wang, D. N. Tafen, J. P. Lewis, Z. Hong, A. Manivannan, M. Zhi, M. Li and N. Wu, *J. Am. Chem. Soc.*, 2009, **131**, 12290.
34 H.-H. Lo, N. O. Gopal and W. S.-C. Ke, *Appl. Phys. Lett.*, 2009, **95**, 083126.
35 O. K. Varghese, M. Paulose, T. J. LaTempa and C. A. Grimes, *Nano Lett.*, 2009, **9**, 731.
36 X. Chen and C. Burda, *J. Am. Chem. Soc.*, 2008, **130**, 5018.